Studies of GPDs at Jefferson Lab: results and future experiments

IOP Conf. Series: Journal of Physics: Conf. Series **938** (2017) 012003 doi:10.1088/1742-6596/938/1/012003

Studies of GPDs at Jefferson Lab: results and future experiments

Angela Biselli
for the CLAS collaboration
Professor, Fairfield University, Fairfield, 06824 CT, USA
E-mail: biselli@jlab.org

Abstract. The Generalized Parton Distributions (GPDs) have emerged as a universal tool to describe hadrons in terms of their elementary constituents, the quarks and the gluons. Deeply Virtual Compton Scattering (DVCS) on a proton or neutron (N), $eN \to e'N'\gamma$, is one of the simplest processes that can be described in terms of GPDs. The amplitudes of DVCS and Bethe-Heitler, process where a photon is emitted by the incident or scattered electron, can be accessed via cross section measurements or exploiting their interference which give rise to spin asymmetries. Spin asymmetries, cross sections and cross-section differences can be connected to different combinations of the four leading order GPDs (H, E, $\tilde{H}$, $\tilde{E}$) for the two quark flavors depending on the observable and the type of target.

1. Introduction

Elastic scattering and deep inelastic scattering have been for years the methods of choice to study the structure of the nucleon. Elastic scattering gives access to the form factors which are related to the transverse spatial distribution of quarks, whereas deep inelastic scattering gives access to parton distributions which are longitudinal momentum and spin distribution of quarks. While both these quantities are important, it is clear that they are a subset of more fundamental quantities which encompass all the dimensions in space and momentum. The generalized parton distributions (GPDs) give fully correlated quark distributions in both coordinate and momentum space. These distributions allow access to crucial information such as the angular momentum distribution of quarks in the nucleon [1, 2, 3].

The cleanest way to access GPDs is via deeply virtual Compton scattering (DVCS), where the virtual photon interacts with a single quark of the nucleon radiating a real photon. As shown in Fig. 1, this exclusive process can be factorized, at high photon virtualities, into a hard scattering part, that can be treated perturbatively, and a nucleon-structure part, parameterized by the GPDs.

At leading twist the soft process is described by four chiral-even GPDs: H, $\tilde{H}$, E, and $\tilde{E}$, which depend on the longitudinal momentum fraction transferred to the proton, $\xi \simeq x_B/(2-x_B)$, the momentum transfer, t, between the virtual and the real photons and the momentum fraction of the struck quark, $x+\xi$, which is not experimentally accessible. All these four GPDs all involve processes that conserve the quark helicity, but while H and $\tilde{H}$ preserve the nucleon helicity, E and $\tilde{E}$ do not. The GPD H (E) is an average over the two possible possible quark-helicity

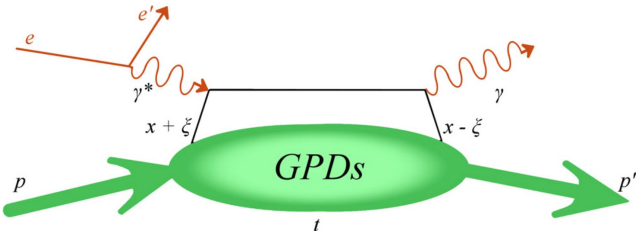

Figure 1. Handbag diagram for the DVCS process.

conserving processes, whereas $\tilde{H}$ $(\tilde{E})$ is a difference. GPDs are defined at the quark level for each flavor.

From the experimental point of view, the DVCS cannot be disentangled from the Bethe Heitler process, where the final-state photon is emitted by either the incoming or the outgoing electron. To extract the DVCS amplitude $T_{\rm DVCS}$, which contains the GPDs, one can measure both cross-section

$$\frac{d^4\sigma}{dQ^2 dx_B dt d\phi} \propto |T_{\rm DVCS} + T_{\rm BH}|^2 = |T_{\rm DVCS}|^2 + |T_{\rm BH}|^2 + I, \tag{1}$$

or asymmetries, which at leading twist can be written as:

$$A = \frac{\sigma^+ - \sigma^-}{\sigma^+ + \sigma^-} \propto \frac{I}{|T_{\rm DVCS}|^2 + |T_{\rm BH}|^2 + I}. \tag{2}$$

Here $I = T_{\rm DVCS} T^*_{\rm BH} + T^*_{\rm DVCS} T_{\rm BH}$ is the interference between the two processes. The DVCS amplitude $T_{\rm DVCS}$ depends on linear combinations of Compton form factors $\mathcal{F}$, whose real and imaginary parts are connected to the GPDs by

$$\Re{\rm e}\mathcal{F} = \mathcal{P} \int_{-1}^{1} dx \left[\frac{1}{x-\xi} \mp \frac{1}{x+\xi} \right] F(x,\xi,t) \tag{3}$$

$$\Im{\rm m}\mathcal{F} = \pi \left[F(\xi,\xi,t) \mp F(-\xi,\xi,t) \right] \tag{4}$$

Here the "$\mp$" sign apply, respectively, to the quark-helicity independent, or unpolarized, GPDs (H, E) and to the quark-helicity dependent, or polarized, GPDs $(\tilde{H}, \tilde{E})$. This means that the experimental observables depend on eight GPD-related quantities. Moreover the CFFs accessed experimentally are not directly the quark ones but CFFs for the type of target, proton, neutron or nuclei, which are linear combination of CFFs of different quark flavors. Luckily different observables (e.g. beam and target asymmetries) and different targets have different sensitivities to the various CFFs and therefore by performing several measurements one can separate the different contributions for a certain target and ultimately, by combining different target measurements one can perform flavor separation. For instance, the beam-spin asymmetry $A_{\rm LU}$ can be expressed as [4]

$$A_{\rm LU}(\phi) \propto \Im{\rm m} \left\{ F_1 \mathcal{H} + \frac{x_{\rm B}}{2 - x_{\rm B}} (F_1 + F_2)(\widetilde{\mathcal{H}} - \frac{t^2}{4M^2} F_2 \mathcal{E}) + ... \right\} \sin\phi\,, \tag{5}$$

where F_1 and F_2 are the form factors, and is sensitive to $\mathcal{H}$, $\tilde{\mathcal{H}}$, and $\mathcal{E}$, particularly to $\mathcal{H}_p$ for the proton and to $\mathcal{E}_n$ for the neutron. The longitudinal target-spin asymmetry $A_{\rm UL}$

$$A_{\rm UL}(\phi) \propto \Im{\rm m} \left\{ F_1 \widetilde{\mathcal{H}} + \frac{x_{\rm B}}{2 - x_{\rm B}} (F_1 + F_2)(\mathcal{H} + \frac{x_{\rm B}}{2} \mathcal{E}) + ... \right\} \sin\phi\,, \tag{6}$$

is equally sensitive to $\mathcal{H}_p$ and $\tilde{\mathcal{H}}_p$ for the proton and $\mathcal{H}_n$ for the neutron. Furthermore the cross section and the double spin asymmetry are sensitive to the real part CFFs.

2. Results

This paper focuses on the last decade DVCS results at Jefferson Lab from Hall A and Hall B and the future measurements planned at this facility (see Section 3). Jefferson lab operated at a maximum energy of 6 GeV, a much lower energy as compared to other facilities, which allows to access the large x_{B} region and therefore have an insight into the quarks valence region. Hall A used a high resolution spectrometer to detect the electron and an electromagnetic calorimeter to detect the photon, while the presence of the proton or neutron was ensured via missing mass cuts. Hall B used the CEBAF Large Acceptance Spectrometer (CLAS) [5] in its standard configuration with an additional calorimeter (inner calorimeter) for the detection of forward photons. In this configuration the complete final state $ep\gamma$ was simultaneously detected and its exclusivity was ensured by applying a set tight kinematic cuts. CLAS is a large acceptance detector which allowed to measure the DVCS process over a large kinematic range in Q^2, x_{B} and t, providing rich data sets to explore the GPD dependence on such variables. Experiments conducted at Jefferson Laboratory includes measurements of asymmetries and cross sections on protons, neutrons and nuclei

2.1. Asymmetries

The most accessible quantities that can be measured to study DVCS are the beam and target spin asymmetries, BSA and TSA respectively. These quantities depend on the interference between BH and DVCS and therefore show a clear DVCS signal. Also, by virtue of the fact that asymmetries are a ratio, they are less sensitive to certain systematic effects, albeit they have much larger statistical uncertainties than cross sections. Two exploratory measurements in Hall B of the BSA [6] and TSA [7] showed the handbag dominance and a clear twist-2 $\sin\phi$ dependence and triggered a series of dedicated experiments with both unpolarized and polarized targets focused on the extraction these asymmetries over a large kinematic range [8, 9, 10]. For example, Figure 2 shows the $-t$-dependence of the $\sin\phi$ term of the BSA [10] and TSA [9]. The proton BSA, sensitive to $\Im\mathrm{m}\mathcal{H}_p$, shows a steeper drop than $\Im\mathrm{m}\widetilde{\mathcal{H}}_p$. Since the Compton form factors $\Im\mathrm{m}\mathcal{H}_p$ and $\Im\mathrm{m}\widetilde{\mathcal{H}}_p$ are related to the Fourier transforms of the electric charge and axial charge respectively, this behavior indicates that the axial charge is more concentrated in the proton center than the electric one.

Using the polarized proton data, the double spin asymmetry (DSA) was also measured [10]. The DSA is important since it provides information on the real part of the Compton form factors but conversely to the single spin asymmetries it has a large BH component. The measurement of the three asymmetries at the same kinematic points allowed a simultaneous fit to extract the Compton form factors for the proton. This was done using a quasi model-independent technique [15] in which the bounds of the domains of variation of the CFFs is limited to ±5 times the value predicted by the VGG model [11], and $\widetilde{\mathcal{E}_p}$=0. Figure 3 shows the results of the fit for $\Im\mathrm{m}\mathcal{H}_p$ and $\Im\mathrm{m}\widetilde{\mathcal{H}}_p$. In addition to confirming the fact that the axial charge is more concentrated than the electrical charge, one can see that the slope of $\Im\mathrm{m}\mathcal{H}_p$ decreases as x_{B} becomes bigger, indicating that the electric charge is more concentrated for valence quarks than sea quarks.

In Hall B Tthe BSA on nuclei was also measured [16]. The experiment used a ^{4}He target, which being a spin-0 nucleus at twist-2 is sensitive only to the GPD H_A. The analysis measured the BSA for coherent ($e^4\mathrm{He} \rightarrow e^4\mathrm{He}\gamma$) scattering which was used to extract, in a model-independent way, the real and the imaginary parts of the ^{4}He CFF, H_A providing a first insight on the partonic structure of nuclei.

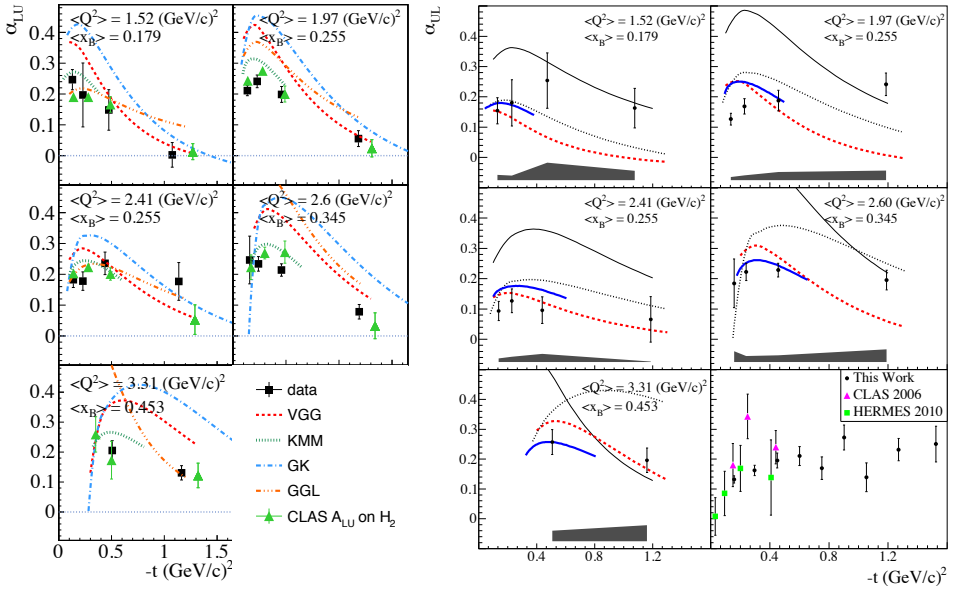

Figure 2. BSA (left panel) and TSA (right panel) $-t$ dependence of the $\sin\phi$ term. Left panel: the curves show the VGG prediction [11] (red dashed), KMM12 [12] (green dotted), GK [13] (blue dash-dotted), and GGL [14] (orange dashed-three- dotted). The triangular green data come from the previous CLAS experiment with unpolarized proton target [8]. Right panel: the curves show the predictions of 4 GPDs models: VGG (red dashed line), GK (black dotted lube), KMM12 (blue thick solid line), GGL (black solid line). The data agree qualitatively with the model predictions but clearly provide new constraints to the GPDs. More details on the models comparison can be found in [10, 9]

2.2. Cross-sections, and cross section differences

Cross sections and cross section differences are essential to measure with high precision the real part of Compton form factors. Both Hall A and Hall B have extracted cross sections with a proton target. In all these experiments the beam was polarized allowing the extraction of the cross section differences as well. Hall A results from 2006 [17] and the recent re-analysis of the same dataset [18] extracted the cross section and the cross-section differences over a limited Q^2 and $-t$ with high precision. A fit of the data allowed to extract both the DVCS and interference Compton form factor, as well as twist-2 and twist-3 contributions. The same Hall B experiment that lead to the first dedicated measurement of BSA [8] was analyzed to extract the cross sections and cross-section differences over a large kinematic range [19]. Results of this work show a clear non-zero contribution from the DVCS process. Moreover, using [15] the real and imaginary part of $\mathcal{H}$ was found with $\mathcal{E}_p$ and $\widetilde{\mathcal{E}}_p$ set to zero. The $x_{\rm B}$ trend of the fit indicate that the transverse size and partonic content are bigger at smaller momentum fractions. Additional data with polarized beam on unpolarized protons was taken in 2008-2009. This data was not included in either [8] and [19] and they were analyzed independently [20]. Preliminary results of cross-sections and cross-sections difference are shown in Figure 4. The publication of these results is currently in preparation and it will provide new constraints to the GPDs fits.

Hall A has recently published new results on cross-section and cross-section differences [21]. In this work data were taken at different beam energies and, leveraging the beam energy dependence on the various factors that multiply cross section contributions, a Rosenbluth separation was performed to separate the $|T_{DVCS}|^2$ from the $DVCS$-BH interference I amplitudes. Figure 5 shows a sample of the cross section and cross section differences results (right two panels) and

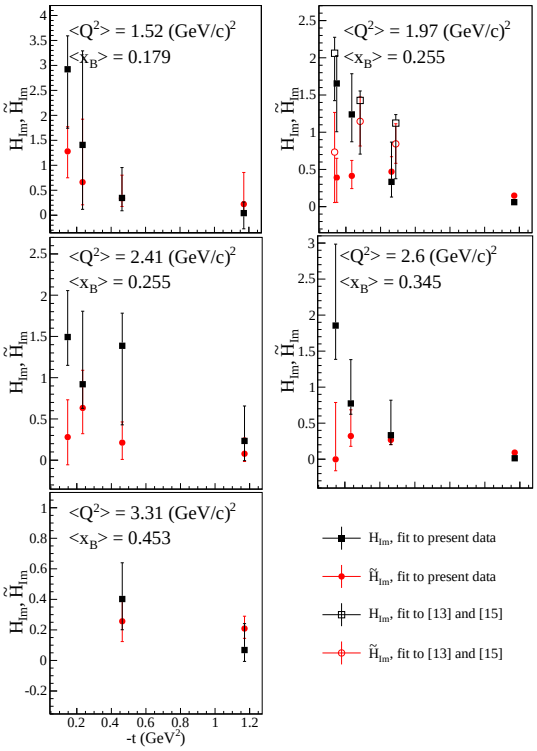

Figure 3. Compton form factor extraction from the simultaneous fit of BSA, TSA and DSA. The solid black squares and the solid red circles show the results for the imaginary parts of $\mathcal{H}_p$ and $\widetilde{\mathcal{H}}_p$ respectively. The results are compared to fits to previous CLAS data [7, 8]

the results for the separation of the amplitudes (left two panels). One can see the high sensitivity of the data to the higher twist (HT) or next-to-leading order (NLO) and therefore to the gluons contributions.

Cross-section and cross-section difference were also extracted for the neutron [22]. Neutron measurements are essential since they are needed, once combined with the proton measurements, to do flavor separation. The $\sin\phi$ moment for the neutron, which is sensitive to $\mathcal{E}_n$ was found very small, nevertheless comparison with models where different values of the angular momentum of the u and d quarks, shows that the data are sensitive to this quantity.

3. Future experiment

The experimental program at Jefferson lab on DVCS has been producing numerous compelling results. Compton form factors for proton, neutron and helium were extracted in several kinematic bins offering a first insight on the distribution of the electric and axial charge for valence and sea quark and hopefully to extract the angular momentum of the d and u quarks. To have a full picture of the GPDs, more data are needed. The Continuous Electron Beam Accelerator Facility (CEBAF) facility has been upgraded to a maximum of beam energy of 12 GeV. In addition to the new experimental Hall, Hall D, focusing mostly on hadron spectroscopy, the detectors in the three existing halls have been upgraded as well to perform at the new maximum energy. Hall A and C still host high resolution spectrometers while Hall B upgraded its detector to the so called CLAS12. Similarly to its predecessor, CLAS12 features six superconducting coils which define six sectors, each equipped with three regions of drift chambers, a high and a low threshold Cherenkov detector, a pre-shower and a electromagnetic

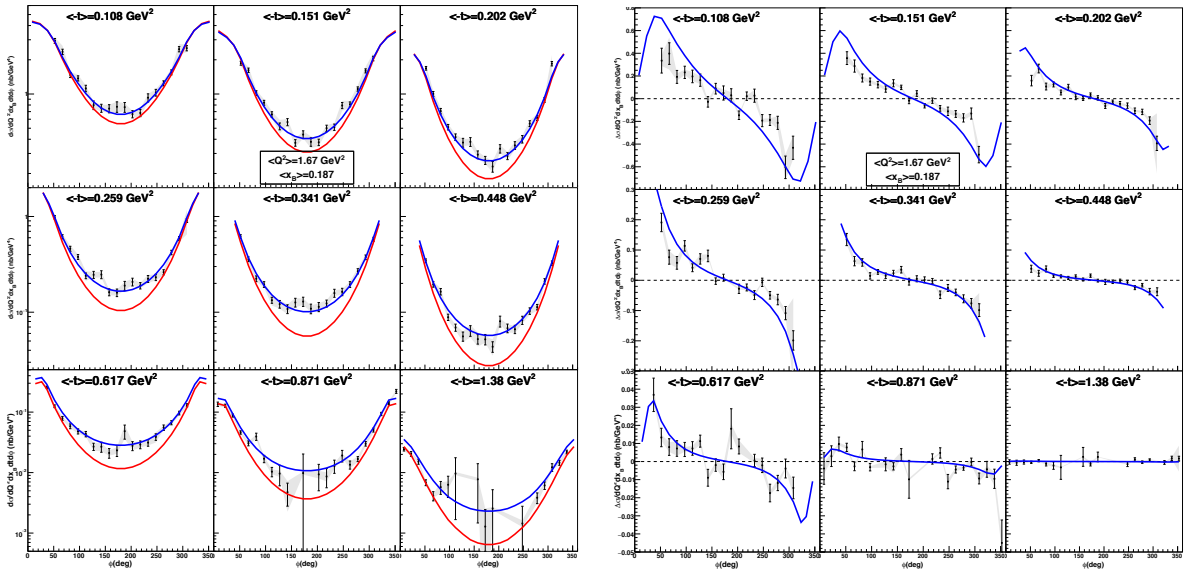

Figure 4. The unpolarized cross section (left) and cross-section differences (right) as a function of ϕ for the Bx=0.187 GeV^2 and Q^2=1.67 GeV^2. The blue curve is the result of the the VGG model and the the red (only left panel) is BH only. The grey band represents the systematic uncertainty.

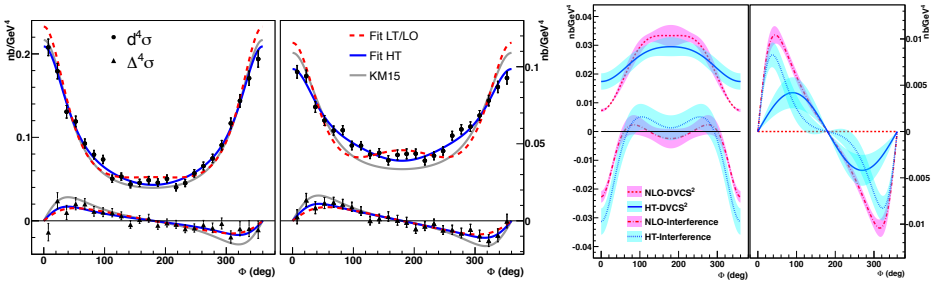

Figure 5. Cross sections and cross-section differences at Q^2=1.75 GeV^2, Bx=0.36, and t = 0.30 GeV^2 for two different beam energies (left). Dashed lines represent the LT/LO fit, solid blu lines is the HT fit. $|T_{DVCS}|^2$ and DVCS-BH interference I contributions for cross section and cross-section differences (right).

calorimeter and a forward time-of-flight scintillators. The new spectrometer has also a central detector around the target which allows the detection of particles at large angles. The central detector consist of a solenoid magnet, a silicon vertex tracker and the central time-of-flight. CLAS12 is shown in left panel of Figure 6. The right panel of Figure 6 shows the kinematic coverage (Q^2 vs x_B) of Jefferson lab as compared to other facilities. As one can see Jefferson lab is uniquely suited to study the valence quark region (high x_B) and the large acceptance of CLAS12 will allow mapping of the GPDs up to a $x_{\rm B} = 0.65$. There are several experiments dedicated to the DVCS program in all three experimental halls. The first experiment has taken already data in Hall A and focused on extracting the beam polarized and unpolarized cross sections on the proton. The experiment will run at three different beam energies and will extract the $|T_{DVCS}|^2$ term via Rosenbluth separation similarly to [21]. This experiment will be followed in Fall 2017 by the first CLAS12 experiment, which will focus on the extraction of the DVCS beam spin

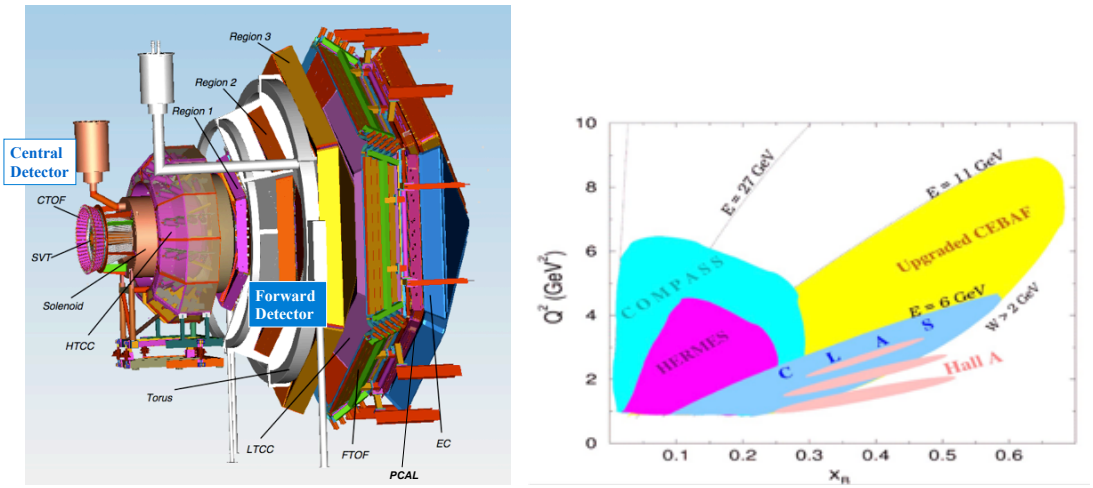

Figure 6. CLAS12 (left) and Jefferson Laboratory kinematic range (right).

asymmetry and cross section on the proton. Other experiments are planned in the following years to measure target and double spin asymmetries on the proton and to conduct the same measurements on the neutron. Figure 7 shows a sample of the expected results for the target spin asymmetry of the neutron. Moreover proposals to measure DVCS at different energies and using the transverse target with CLAS12 have been approved. This set of experiments represent a comprehensive study of the DVCS on both proton and neutron and the completion of such program will give a first insight on quarks' GPDs and, possibly, will allow the testing of Ji sum's rule.

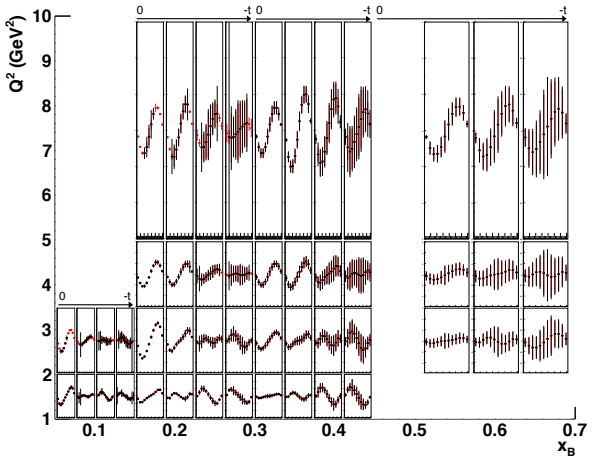

Figure 7. Projected target-spin asymmetry. The y-scale range, common to all bins, is -0.6-0.6. The black and red points are obtained, respectively, without and with the Forward Tagger.

References

[1] D. Mueller, D. Robaschik, B. Geyer, F. M. Dittes and J. Horejsi, Fortsch. Phys. **42**, 101 (1994).
[2] X. D. Ji, Phys. Rev. Lett. **78**, 610 (1997).
[3] A. V. Radyushkin, Phys. Rev. D **56**, 5524 (1997).

[4] A. V. Belitsky, D. Mueller and A. Kirchner, Nucl. Phys. B **629**, 323 (2002).
[5] B. A. Mecking *et al.* [CLAS Collaboration], Nucl. Instrum. Meth. A **503**, 513 (2003).
[6] S. Stepanyan *et al.* [CLAS Collaboration], Phys. Rev. Lett. **87**, 182002 (2001)
[7] S. Chen *et al.* [CLAS Collaboration], Phys. Rev. Lett. **97**, 072002 (2006).
[8] F. X. Girod *et al.* [CLAS Collaboration], Phys. Rev. Lett. **100**, 162002 (2008).
[9] E. Seder *et al.* [CLAS Collaboration], Phys. Rev. Lett. **114**, no. 3, 032001 (2015)
[10] S. Pisano *et al.* [CLAS Collaboration], Phys. Rev. D **91**, no. 5, 052014 (2015).
[11] M. Vanderhaeghen, P. A. M. Guichon and M. Guidal, Phys. Rev. D **60**, 094017 (1999); M. Guidal, M. V. Polyakov, A. V. Radyushkin and M. Vanderhaeghen, Phys. Rev. D **72**, 054013 (2005).
[12] K. Kumericki, D. Muller and M. Murray, Phys. Part. Nucl. **45**, no. 4, 723 (2014).
[13] P. Kroll, H. Moutarde and F. Sabatie, Eur. Phys. J. C **73**, no. 1, 2278 (2013).
[14] G. R. Goldstein, J. O. Hernandez and S. Liuti, Phys. Rev. D **84**, 034007 (2011).
[15] M. Guidal, Eur. Phys. J. A **37**, 319 (2008).
[16] M. Hattawy *et al.*, arXiv:1707.03361 [nucl-ex].
[17] C. M. Camacho *et al.* [Jefferson Lab Hall A and Hall A DVCS Collaborations], Phys. Rev. Lett. **97**, 262002 (2006).
[18] M. Defurne *et al.* [Hall A Collaboration], arXiv:1504.05453 [nucl-ex].
[19] H. S. Jo *et al.* [CLAS Collaboration], arXiv:1504.02009 [hep-ex].
[20] N. Hirlinger Saylor. *in preparation.*
[21] M. Defurne *et al.*, arXiv:1703.09442 [hep-ex].
[22] M. Mazouz *et al.* [Jefferson Lab Hall A Collaboration], Phys. Rev. Lett. **99**, 242501 (2007) doi:10.1103/PhysRevLett.99.242501